RAPID COMMUNICATIONS

PHYSICAL REVIEW A VOLUME 30, NUMBER 5 NOVEMBER 1984

Hyperfine structure of N_2 ($B\,^3\Pi_g$ and $A\,^3\Sigma_u^+$): Oscillatory J dependence of the $^3\Pi_{0,1}$ hyperfine structure

H. Geisen, D. Neuschäfer, Ch. Ottinger, and A. Sharma*
Max-Planck-Institut für Strömungsforschung,
D-3400 Göttingen, Federal Republic of Germany
(Received 27 July 1984)

Laser-induced fluorescence on a beam of metastable N_2 ($A\,^3\Sigma_u^+$) molecules has been used to study the hyperfine structure of the (10,6) band of the N_2 (B-A) transition. The hyperfine structure of the $B\,^3\Pi_0$ and $^3\Pi_1$ states was found to have an unusual, oscillatory J dependence. This was explained by perturbation theory, and hyperfine-structure constants for the B state were derived from a data fit. At the same time results from earlier, less-direct experiments on the A-state hyperfine structure were confirmed and extended.

Using sub-Doppler laser spectroscopy, the hyperfine structure (hfs) of molecular transitions can be resolved. We have done hfs measurements on the (10,6) band of the N_2 ($B\,^3\Pi_g$-$A\,^3\Sigma_u^+$) system by laser-induced fluorescence (LIF), crossing a beam of metastable N_2 (A) molecules at right angles with a dye laser beam. A very unusual hfs of the $B\,^3\Pi_0$ and $^3\Pi_1$ states was found, exhibiting an oscillatory dependence on J. This contrasts with the much more regular hfs of the A state, which is known from earlier, Rabi-type experiments on a beam of N_2 (A) (Refs. 1 and 2), but was determined in the present work for a much greater number of J levels.

N_2 (A) molecules were prepared by striking a dc discharge ~ 2 A directly in an N_2 nozzle beam, using the nozzle itself as an anode. With a nozzle temperature of 720 K, nozzle diameter of 1 mm, and a backing pressure of 30 Torr, a rotational temperature of 315 K for N_2 ($A, v=6$) was measured by LIF. About 300 lines of the (10,6) band of N_2 (B-A) were recorded on a strip chart and were identified using molecular constants from the literature.[3] Using very slow (~ 1 MHz/sec) laser scan speeds, the hfs of all lines was measured with a resolution of up to 15 MHz full width at half maximum (FWHM), and with very good S/N ratio. The hfs splittings were determined using an interferometer with a 62.5-MHz free spectral range.

As an example, Fig. 1 shows the hfs pattern of the $Q_{33}(2)$ line; 11 of the expected 13 components are resolved. All distinguishable hfs components of all measured lines were identified, on the basis of the $\Delta F=0, \pm 1$ selection rule and the approximate proportionality between line intensities and F values. hfs level splittings of both the N_2 (B) and N_2 (A) states were then derived from the measured splittings of the lines.

Figures 2 and 3 show the results. The level separations, as a function of J, are plotted relative to the central component (having $F=J$), which is shown as a horizontal line. The estimated accuracy of the data is ± 2 MHz. In the N_2 (A) state, Fig. 2, hfs splittings of the F_1 and F_3 fine-structure terms (regular and inverted, respectively) tend to a constant limit with increasing J, while the F_2 term shows a measurable hfs only for the lowest J. The hfs of N_2 ($B, ^3\Pi_{0,1,2}$) Fig. 3, is very striking: For $^3\Pi_2$, the splitting decreases monotonically, and in the same way for *ortho*-N_2 and *para*-N_2. For $^3\Pi_0$, levels with no detectable splitting alternate with levels which are split. For *ortho*-N_2, levels with even J are split; for *para*-N_2, those with odd J are split. Here the magnitude of the splitting increases with J. Finally, $^3\Pi_1$ is intermediate between $^3\Pi_2$ and $^3\Pi_0$.

For N_2 (A), the hfs coupling constants and matrix elements given in Refs. 1 and 2 show that, by far, the most important contribution comes from the magnetic interaction [Eq. (A12) in Ref. 1]. From this expression, one obtains the energy separations between levels F and $F-1$ of the F_1, F_2, F_3 terms [Eqs. (1), (2), and (3), respectively]

$$\Delta E = c_0^2 (F/J)[\alpha - \beta(2J-2)/(2J+1)] + 3c_0c_1F[J(J+1)]^{-1/2}[\beta/(2J+1)][(2J+3)/(2J+1)]^{1/2} , \quad (1)$$

$$\Delta E = F/[J(J+1)](\alpha + 2\beta) , \quad (2)$$

$$\Delta E = -c_0^2[F/(J+1)][\alpha - \beta(2J+4)/(2J+1)] + 3c_0c_1F[J(J+1)]^{-1/2}[\beta/(2J+1)] . \quad (3)$$

The coefficients $c_0=[(R+\delta)/(2R)]^{1/2}$ and $c_1=[(R-\delta)/(2R)]^{1/2}$ describe the contributions of wave functions with $N=J+1$ and $N=J-1$ [Ref. 1, Eqs. (11)–(15)] to the wave function appearing in Ref. 1, Eq. (A12). Here, $R=(\delta^2+4X^2)^{1/2}$, with

$$\delta = 2B(2J+1) - 2\lambda/(2J+1)$$

and

$$X = 2\lambda[J(J+1)]^{1/2}/(2J+1) ,$$

where $\lambda=-1.2935$ cm^{-1}, $B=1.3345$ cm^{-1}. The constants $\alpha=12.657\pm0.013$ MHz and $\beta=-12.540\pm0.009$ MHz for N_2 ($A, v=6$) are given in Ref. 2 and describe the Fermi contact and the dipolar interaction, respectively. The dashed curves in Fig. 2 were calculated from Eqs. (1)–(3), and are seen to fit our data very well, over a much wider range of J levels than were studied in Ref. 1.

In the $B\,^3\Pi_g$ state, we again consider only magnetic hfs interactions. hfs formulas for Hund's case (a) are given in Ref. 4. One important conclusion is that a $^3\Pi_0$ state should

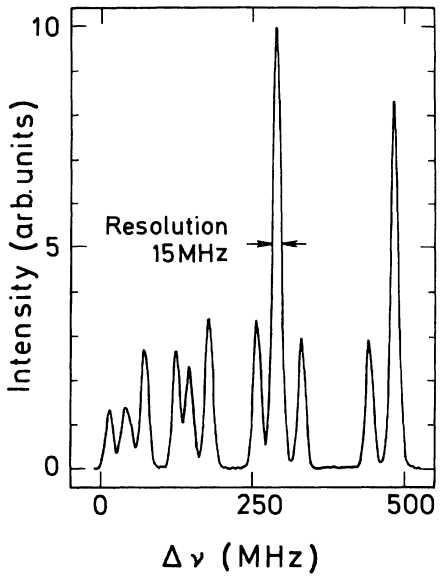

FIG. 1. Hyperfine splitting of the $Q_{33}(2)$ line of the N_2 $(B\text{-}A)$, (10,6) band at 17145.03 cm^{-1}.

not have any magnetic hfs at all. Our observation (Fig. 3), therefore, indicates that the $^3\Pi_0$ wave functions are not purely case (a), but are perturbed by the molecular rotation. The rotation Hamiltonian $B(\vec{J}-\vec{L}-\vec{S})^2$ perturbs the "pure" Hund's case (a) wave functions $|\Omega\rangle$, to give in first order[5] [with $x=J(J+1)$],

$$|\psi^{\pm}\rangle_{\Omega=0}=|0^{\pm}\rangle-(B/A)(2x)^{1/2}|1^{\pm}\rangle\ , \tag{4}$$

$$|\psi^{\pm}\rangle_{\Omega=1}=|1^{\pm}\rangle+(B/A)(2x)^{1/2}|0^{\pm}\rangle -(B/A)(2x-4)^{1/2}|2^{\pm}\rangle\ , \tag{5}$$

$$|\psi^{\pm}\rangle_{\Omega=2}=|2^{\pm}\rangle+(B/A)(2x-4)^{1/2}|1^{\pm}\rangle\ . \tag{6}$$

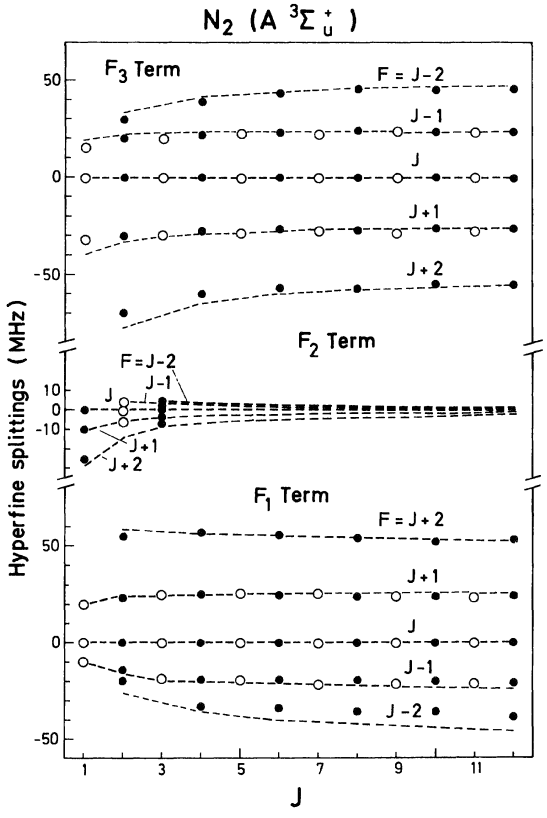

FIG. 2. Hyperfine splitting of the N_2 $(A, v=6)$ levels. Dots (o-N_2) and circles (p-N_2) are measured, dashed lines are calculated.

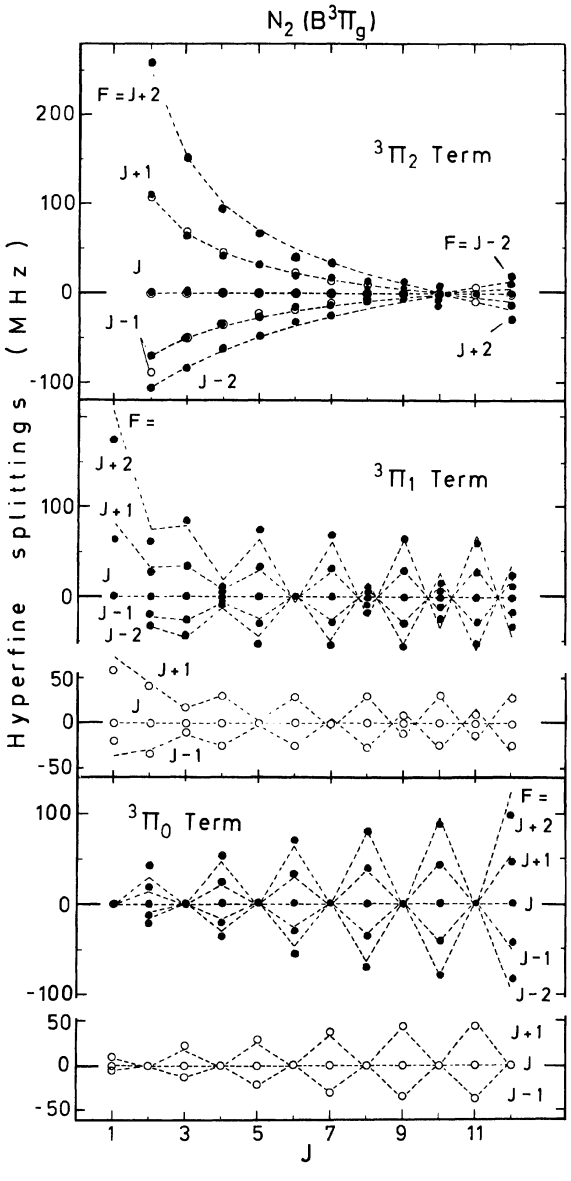

FIG. 3. Same as Fig. 2, for N_2 $(B, v=10)$. In the $^3\Pi_2$ term the hfs is almost identical for o-N_2 and p-N_2.

$B = 1.44098\ \text{cm}^{-1}$ is the rotational constant and $A = 41.525\ \text{cm}^{-1}$ is the spin-orbit coupling constant of N_2 ($B, v = 10$) (Ref. 3), and $|\Omega^{\pm}\rangle \equiv [|\Omega\rangle \pm |-\Omega\rangle]/\sqrt{2}$. In Ref. 4, hyperfine matrix elements for the nonparity states $|\Omega\rangle$ and $|-\Omega\rangle$ are given. From Ref. 4, Eq. (3) and Table II, one obtains the following matrix elements between the parity states $|\Omega^{\pm}\rangle$:

$$\langle 2^{\pm}|H|2^{\pm}\rangle = y(2/\sqrt{6})[2D_{11}/\sqrt{30} + \sqrt{6}G_{11} + K_{11}] \ , \quad (7)$$

$$\langle 2^{\pm}|H|1^{\pm}\rangle = y[(x-2)/12]^{1/2}[D_{11}/\sqrt{30} - K_{11}] \ , \quad (8)$$

$$\langle 1^{\pm}|H|1^{\pm}\rangle = yG_{11} \ , \quad (9)$$

$$\langle 1^{\pm}|H|0^{\pm}\rangle = y(x/12)^{1/2}[D_{11}/\sqrt{30} - K_{11} \mp D_{1-1}/\sqrt{5}] \ , \quad (10)$$

$$\langle 0^{\pm}|H|0^{\pm}\rangle = 0 \ . \quad (11)$$

H is the hyperfine Hamiltonian including only magnetic dipole terms [the quadrupole interaction would, e.g., give a nonvanishing term in Eq. (11)], and

$$y = [F(F+1) - I_T(I_T+1) - J(J+1)]/[2J(J+1)] \ ,$$

with the total nuclear spin I_T. G_{11}, K_{11}, D_{11}, and D_{1-1} are molecular parameters describing the nuclear spin-orbit interaction (G_{11}), the Fermi contact interaction (K_{11}), and the dipolar interaction (D_{11} and D_{1-1}) for each nucleus separately, as defined in Ref. 4, Table II [the label (1) used in Ref. 4 to indicate nucleus 1 has been dropped for brevity]. The energies (7)–(11) include factors of 2 from the summation over both nuclei.

The diagonal matrix elements of the perturbed states, $\langle \psi^{\pm}|_{\Omega=0,1,2} H |\psi^{\pm}\rangle_{\Omega=0,1,2}$, are obtained from the expressions (4)–(6), using (7)–(11). Keeping only terms linear in B/A, we then find the energy differences between terms F and $F-1$, in the $\Omega = 2$ case,

$$\Delta E = (F/x)\{2G_{11} + 4D_{11}/(3\sqrt{20}) + \sqrt{6}K_{11}/3 + (B/A)(x-2)[2D_{11}/(3\sqrt{20}) - \sqrt{6}K_{11}/3]\} \ . \quad (12)$$

This splitting obeys the Landé interval rule, and decreases essentially as $1/J$ in the limit of large J, in agreement with the observation (Fig. 3, top).

Similarly for the $^3\Pi_0$ state, one finds the energy differences between the diagonal elements F and $F-1$:

$$\Delta E = (FB/A)[\pm 2D_{1-1}/\sqrt{30} - 2D_{11}/(3\sqrt{20}) + \sqrt{6}K_{11}/3] \ . \quad (13)$$

Thus the zero-order term makes no contribution to the hfs. The splitting results solely (in our approximation) from the perturbation of $^3\Pi_0$ by $^3\Pi_1$. It has the interesting property of being of different magnitude for the $|\psi^+\rangle$ and $|\psi^-\rangle$ states. These correspond to the two Λ doublet components of each $^3\Pi_0 J$ level. The extremely small hfs splitting for alternate J levels, of a given N_2 modification (Fig. 3, bottom) can then be associated with the subtractive combination of the constants in Eq. (13). [The constants given in Eq. (15) happen to be such that for these levels, an overall $\Delta E \lesssim 3$ MHz results.] The other levels of the same modification will then have an additive combination of terms and a large splitting, as is in fact observed. For a given J, the two modifications are associated with opposite signs in $|\Omega^{\pm}\rangle$ and $|\psi^{\pm}\rangle$, which explains the out-of-phase oscillation of the hfs for *ortho*-N_2 and *para*-N_2.

Finally, for the $^3\Pi_1$ state, the hfs energy differences are

$$\Delta E = (F/x)[G_{11} + (B/A)(4D_{11}/(3\sqrt{20}) - 2\sqrt{6}K_{11}/3)] \mp (F2B/A)D_{1-1}/\sqrt{30} \ . \quad (14)$$

This shows clearly the observed decreasing ΔE with increasing J, superimposed by an oscillatory term which increases with F (and J). Note that the oscillations in the $^3\Pi_1$ and $^3\Pi_0$ states are predicted to be out of phase, again in agreement with the observation (Fig. 3, middle and bottom).

From a least-squares fit to all data, the following set of hfs constants was derived for N_2 ($B, v = 10$):

$$G_{11} = 82\ \text{MHz};\ D_{11} = 0\ \text{MHz} \ ; \quad K_{11} = 69\ \text{MHz};\ D_{1-1} = -171\ \text{MHz} \ . \quad (15)$$

Using these constants and Eqs. (12)–(14), the dashed lines shown in Fig. 3 were calculated. The overall fit with the experimental data is very satisfactory; the remaining discrepancies are ascribed partly to the first-order perturbation theory and partly to our neglect of the quadrupole interaction. The first-order treatment alone is not responsible: Excluding from the fit the $J = 9$–12 data points, where this approximation begins to fail, the agreement was only slightly improved. The above constants are therefore only tentative, and a more rigorous analysis is in progress.

This project was supported by the Deutsche Forschungsgemeinschaft.

*Present address: Physics Department, Texas A&M University, College Station, TX 77843.

[1]R. S. Freund, T. A. Miller, D. De Santis, and A. Lurio, J. Chem. Phys. **53**, 2290 (1970).

[2]D. De Santis, A. Lurio, T. A. Miller, and R. S. Freund, J. Chem. Phys. **58**, 4625 (1973).

[3]F. Roux and F. Michaud, J. Mol. Spectrosc. **97**, 253 (1983).

[4]M. Broyer, J. Vigué, and J. C. Lehmann, J. Phys. (Paris) **39**, 591 (1978).

[5]R. N. Zare, A. L. Schmeltekopf, W. J. Harrop, and D. Albritton, J. Mol. Spectrosc. **46**, 37 (1973).